CrossMark

ORIGINAL PAPER

Optimizing the Terzaghi Estimator of the 3D Distribution of Rock Fracture Orientations

Huiming Tang[1] · Lei Huang[1,2] · C. Hsein Juang[2] · Junrong Zhang[1]

Abstract Orientation statistics are prone to bias when surveyed with the scanline mapping technique in which the observed probabilities differ, depending on the intersection angle between the fracture and the scanline. This bias leads to 1D frequency statistical data that are poorly representative of the 3D distribution. A widely accessible estimator named after Terzaghi was developed to estimate 3D frequencies from 1D biased observations, but the estimation accuracy is limited for fractures at narrow intersection angles to scanlines (termed the *blind zone*). Although numerous works have concentrated on accuracy with respect to the blind zone, accuracy outside the blind zone has rarely been studied. This work contributes to the limited investigations of accuracy outside the blind zone through a qualitative assessment that deploys a mathematical derivation of the Terzaghi equation in conjunction with a quantitative evaluation that uses fractures simulation and verification of natural fractures. The results show that the estimator does not provide a precise estimate of 3D distributions and that the estimation accuracy is correlated with the grid size adopted by the estimator. To explore the potential for improving accuracy, the particular grid size producing maximum accuracy is identified from 168 combinations of grid sizes and two other parameters. The results demonstrate that the $2° \times 2°$ grid size provides maximum accuracy for the estimator in most cases when applied outside the blind zone. However, if the global sample density exceeds $0.5°^{-2}$, then maximum accuracy occurs at a grid size of $1° \times 1°$.

Keywords Rock fractures · Fracture orientation · Scanline mapping technique · Terzaghi bias correction · Blind zone · Estimator optimization

1 Introduction

Three-dimensional (3D) fracture geometries have a significant impact on fluid flow and the productivity of geological formations, especially those with low permeability (Ghislain et al. 2016; Nur and Booker 1972). Among the 3D geometric attributes, orientation plays an important role in discrete fracture network (DFN) modeling (Fernandes et al. 2016). The 3D orientation distribution is a fundamental parameter for the DFN hydraulic model, and an accurate estimation of this distribution is essential in the evaluation of gas production and the estimation of fluid flow capabilities in fractured rocks (Middleton et al. 2015; Pandey et al. 2017). Because the 3D structure of a rock system cannot be easily observed, the true 3D fracture geometries, including the orientations, are usually unavailable. However, fresh rock exposures, e.g., outcrops and tunnel pit faces, allow geologists to acquire 2D fracture information through window sampling technique (Mauldon 1998, Mauldon et al. 2001; Han et al. 2016) or 1D fracture information through borehole/scanline mapping technique (Gao et al. 2016; Havaej et al. 2016). In the 1D scanline mapping, bias is often introduced, as fractures with shallow angles of intersection with the scanline are seldom observed (Fisher et al. 2014; Priest 1985).

✉ Lei Huang
huanglei@cug.edu.cn

[1] Department of Geotechnical Engineering and Engineering Geology, Faculty of Engineering, China University of Geosciences, Wuhan 430074, Hubei, China

[2] Glenn Department of Civil Engineering, College of Engineering, Computing and Applied Sciences, Clemson University, Clemson, SC 29634, USA

🖄 Springer

Terzaghi (1965) developed a four-step estimator to estimate the orientation probability distribution in 3D from available 1D biased observations as follows:

1. Partition the projection net into grids of a given size;
2. Count the fracture frequency occurring within each grid;
3. Weight the individual frequencies according to the Terzaghi equation:

$$N_{3D} = \frac{N_{1D}}{\sin \theta} \tag{1}$$

where θ is the intersection angle between the fracture and scanline (Fig. 1a), N_{1D} is the fracture frequency in 1D intersected by the scanline at angle θ, and N_{3D} is the fracture frequency in 3D;

4. Round the weighted frequencies to the nearest integer, because the frequencies defined in this manner must be integers.

The Terzaghi estimator has been widely utilized for 3D orientation distribution estimation in rock relevant fields, such as rock mechanics and hydrocarbon geology (Clair et al. 2015; Haftani et al. 2016; Huang et al. 2016). Previous simulations and practices have demonstrated that the Terzaghi estimator exhibits low accuracy or is simply invalid when applied to fractures at extremely shallow intersection angles to the scanline (Park and West 2002; Priest 1985), and this interval of angle was conceptualized as the blind zone (as shown in Fig. 1b). The size of the blind zone was roughly estimated at 20° (Fouché and Diebolt 2004; Goodman 1976) or 30° (Mauldon and Mauldon 1997; Priest 2012). Although a number of studies have examined the negative effects of the blind zone and its avoidance (Chaminé et al. 2014; Martin and

Tannant 2004; Yow 1987), few researchers have studied the accuracy of the Terzaghi estimator in applications outside the blind zone.

Therefore, this paper focuses on (1) performing a systematic investigation of the accuracy outside the blind zone and (2) exploring potential accuracy improvements. First, a detailed derivation of the Terzaghi equation (Eq. 1) is utilized to qualitatively reveal the source of potential inaccuracy. Next, accuracy magnitudes are quantitatively tested in an experiment employing artificial fractures and involving 168 combined conditions of three parameters: sample density, scanline direction, and grid size. In the experiment, the effect of grid size on the accuracy of the estimator is further examined, and a particular grid size that enables the maximum estimation accuracy is identified to optimize the Terzaghi estimator. Finally, the experiment results are verified using an empirical study of natural fractures in Wenchuan, China.

2 Derivation of the Terzaghi Equation

To reveal potential sources of inaccuracy when applying the Terzaghi estimator outside the blind zone, we must first navigate through the possible theoretical defects of this estimator. A detailed, rigorous mathematical derivation of the Terzaghi equation is employed, although Terzaghi (1965) had given a simple, thin proof for her equation, which was nevertheless insufficient to clarify the theoretical features of the estimator, particularly the possible theoretical defects. For ease of derivation, certain notations are defined first. Based on these notations, the derivation proceeds, using analytic geometry, probability theory, and integrals.
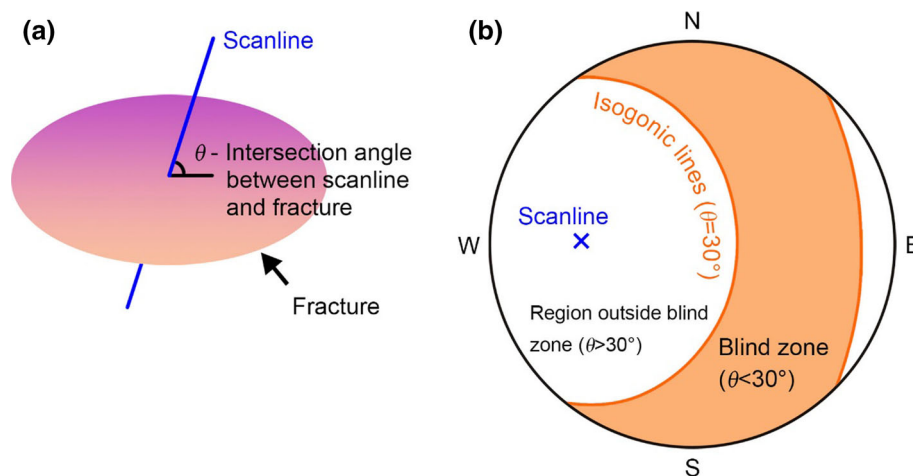
Fig. 1 Illustration of the intersection angle, θ, between the fracture and scanline, the resulting blind zone, and the region of interest outside the blind zone. **a** Intersection angle θ. A fracture is assumed to be disk shaped. An example scanline has a trend/plunge of 090/45°. **b** The blind zone and region of interes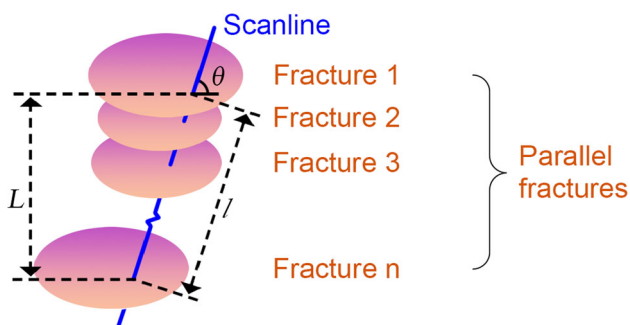t outside the blind zone. They are presented in an equal-angle upper-hemisphere projection. The two isogonic lines are constituted by the poles of those fractures intersected by the scanline at $\theta = 30°$ and define the boundary between the blind zone ($\theta < 30°$) and the region of interest outside the blind zone ($\theta > 30°$)

2.1 Notations

1. Random variable A denotes the orientation of a fracture that occurs in a rock mass (in 3D space).
2. Random variable B denotes the orientation of the fracture intersected by a scanline (in 1D).
3. Set A denotes a collection of random variable A values and represents the collection of orientations of all the fractures in the rock mass.
4. Set B denotes a collection of random variable B values and represents the collection of orientations of those fractures observed with scanline mapping. Set B naturally constitutes a subset of Set A.
5. Set $A \cap B$ denotes the intersection of Sets A and B.
6. $p_A(\alpha, \beta)$ denotes the probability density of random variable A, with α and β representing two elements of orientation: dip direction and dip angle.
7. $p_B(\alpha, \beta)$ denotes the probability density of random variable B.
8. $p_{A \cap B}(\alpha, \beta)$ denotes the probability density of $A \cap B$.
9. $p_{B|A}(\alpha, \beta)$ denotes the conditional probability density of B given A. In probability theory and statistics, the conditional probability density of B given A is defined as the probability density of B when A is known (Kinney 2015). We first consider that A is constant and is interpreted to indicate that all fracture orientations in the rock mass are uniform, or, more generally, that all fractures in the rock mass are parallel. $p_{B|A}(\alpha, \beta)$ accordingly reflects the probability density of the orientations of fractures observed by the scanline under the condition of all fractures being parallel.

2.2 Derivation

For parallel fractures (as shown in Fig. 2), the relationship of the distance (l) between fractures along the scanline to their vertical distance (L) is formulated as follows:

$$l = \frac{L}{\sin \theta} \tag{2}$$

then

$$p_{B|A}(\alpha, \beta) \propto \frac{N}{l} = \frac{N \sin \theta}{L} \tag{3}$$

or equivalently

$$p_{B|A}(\alpha, \beta) = k \sin \theta \tag{4}$$

with

$$k \propto \frac{N}{L} \tag{5}$$

The introduction of $p_{B|A}(\alpha, \beta)$ allows us to connect $p_A(\alpha, \beta)$ and $p_{A \cap B}(\alpha, \beta)$, using the Kolmogorov formula, as follows:

$$p_A(\alpha, \beta) = \frac{p_{A \cap B}(\alpha, \beta)}{p_{B|A}(\alpha, \beta)} \tag{6}$$

An arbitrary orientation region from a projection net (labeled as R, shown in Fig. 3) is partitioned by the Terzaghi estimator into the desired number of grids: σ_1, σ_2, σ_3,..., σ_n. The 3D frequency of orientation in the region R is regarded as the sum of the frequencies over the corresponding grids σ_1, σ_2, σ_3,..., σ_n:
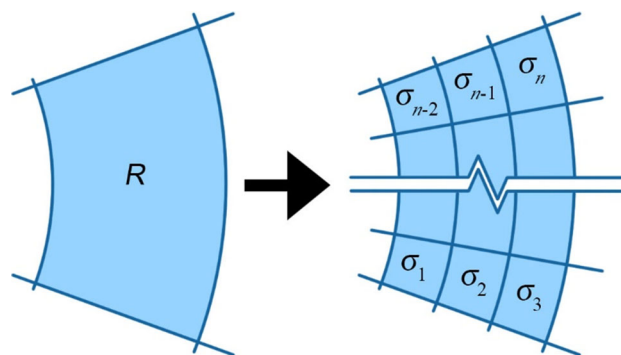
$$\iint_R p_A(\alpha, \beta) \, d\alpha d\beta = \sum_{i=1}^{n} \iint_{\sigma_i} p_A(\alpha, \beta) \, d\alpha d\beta \tag{7}$$

Substituting Eqs. 4 and 6 into Eq. 7 gives

$$\iint_R p_A(\alpha, \beta) \, d\alpha d\beta = \frac{1}{k} \sum_{i=1}^{n} \iint_{\sigma_i} \frac{p_{A \cap B}(\alpha, \beta)}{\sin \theta} \, d\alpha d\beta \tag{8}$$

As noted earlier, Set B is a subset of Set A. Therefore,

$$A \cap B = B \tag{9}$$

Substituting Eq. 9 into Eq. 8 gives

Fig. 2 Intersection between the scanline and parallel fractures at angle θ. The vertical distance between fractures 1 and n is assumed to be L, and their distance along the scanline is assumed to be l

Fig. 3 Example showing the partition of an arbitrary orientation region into grids

$$\iint_R p_A(\alpha, \beta) \mathrm{d}\alpha \mathrm{d}\beta = \frac{1}{k} \sum_{i=1}^{n} \iint_{\sigma_i} \frac{p_B(\alpha, \beta)}{\sin \theta} \mathrm{d}\alpha \mathrm{d}\beta \qquad (10)$$

Suppose that θ_{ci} is the intersection angle between the scanline and fracture defined at the center of grid σ_i ($i = 1$, ..., n) and P_i is the observed 1D frequency over grid σ_i. According to the Riemann middle sum interpretation of the double integral, as described in Peterson (2016), Eq. 10 is rewritten as follows:

$$\iint_R p_A(\alpha, \beta) \mathrm{d}\alpha \mathrm{d}\beta = \varepsilon + \frac{1}{k} \sum_{i=1}^{n} \frac{P_i}{\sin \theta_{ci}} \qquad (11)$$

with

$$\varepsilon = \begin{cases} \neq 0, & \text{if } n < \infty \\ 0, & \text{if } n = \infty \end{cases} \qquad (12)$$

where $\int_R p_A(\alpha, \beta) \mathrm{d}\alpha \mathrm{d}\beta$ is the true 3D frequency in terms of the integral; $\frac{1}{k} \sum_{i=1}^{n} \frac{P_i}{\sin \theta_{ci}}$ is the 3D frequency estimated using the Terzaghi estimator, or in integrals is called the Riemann middle sum; and ε is the Riemann middle sum error, or defined here as the estimation error of the Terzaghi estimator.

Equation 11 is consistent with the Terzaghi (1965) equation, as given in Eq. 1. The error term (as given in Eq. 12) indicates that the Terzaghi estimator does not involve an estimation error if and only if the grid number is infinitely great, or, equivalently, grids are infinitesimal; any other case involves estimation error. In reality, a grid is not infinitesimal, and the Terzaghi estimator consequently involves an estimation error. An alternative interpretation of the error from the spatial geometric viewpoint is that all nonparallel fractures in grid σ_i are incorrectly assumed to be parallel fractures with a uniform orientation, as constrained at the center of the grid (Fig. 4).

3 Fractures Simulation

The purpose of the simulation is to (a) test the accuracy magnitude of the Terzaghi estimator in application outside the blind zone and (b) explore potential accuracy improvements if the accuracy magnitude is low. In our exploration, we examine the effect of grid size on the accuracy and identify the grid size that generates the highest estimation accuracy. This size is then considered the optimal Terzaghi estimator parameter to maximize accuracy.

The simulation employs DFN modeling to connect true 3D and observed 1D distributions, and it subsequently estimates 3D distributions from observed 1D distributions by executing the Terzaghi estimator. In this way, the link between true 3D distributions and estimated 3D distributions can be tested. The accuracy based on the statistical difference between true and estimated 3D distributions is evaluated using the two-dimensional Kolmogorov–Smirnov test. This nonparametric statistical test assesses whether two sets of two-dimensional data come from the same or different distributions. The null hypothesis is that both data sets are sampled from the same continuous distribution. This test returns an asymptotic significance to measure statistical difference. The asymptotic significance ranges between 0 and 1, and a higher asymptotic significance corresponds to a smaller statistical difference and a higher accuracy. Additional information on this test is provided by Justel et al. (1997), Lopes (2010), and Lopes et al. (2007).

The variables in the simulation include the scanline directions, global sample densities, and grid sizes. For a given fracture set, the scanline direction determines the intersection angles from the fractures to the scanline. The required intersection angles can be produced by adjusting the scanline direction. The grid size is the grid dimension assigned in the Terzaghi estimator, and it is directly related to the estimate; see the Terzaghi estimator description in Sect. 1. The global sample density is defined as the average size of the fracture sample per grid size in the projection net. For a given fracture set, the global sample density is dependent on the sample size and thus is relevant to the field survey. The three variables describe custom configurations associated with the field observations and estimations and are potential influencing factors for the accuracy of the Terzaghi estimator. Broad combinations of the three variables values are designed so as to flexibly represent most real situations.

3.1 Analysis Methodology

The simulation follows the three-step process below (see also Fig. 5 for workflow), with the first step specifying the model parameters, the second step realizing the models and 1D orientation observations, and the third step estimating the 3D orientation distribution from 1D observations and evaluating the asymptotic significance.

First, the true 3D distribution of orientations is specified, along with the other parameters necessary for modeling (Table 1). In order to confine the orientations within the region outside the blind zone, a distribution type with upper and lower limits is required. An ideal type having this feature is uniform distribution. Although uniform distribution is not common for orientation distribution characterization, almost all distribution types, including the most frequently applied Fisher distribution, can be flexibly approximated as a piecewise distribution, where each piecewise unit is uniformly distributed at intervals. Hence, analyses based on a piecewise uniform distribution should be sufficiently adaptable.
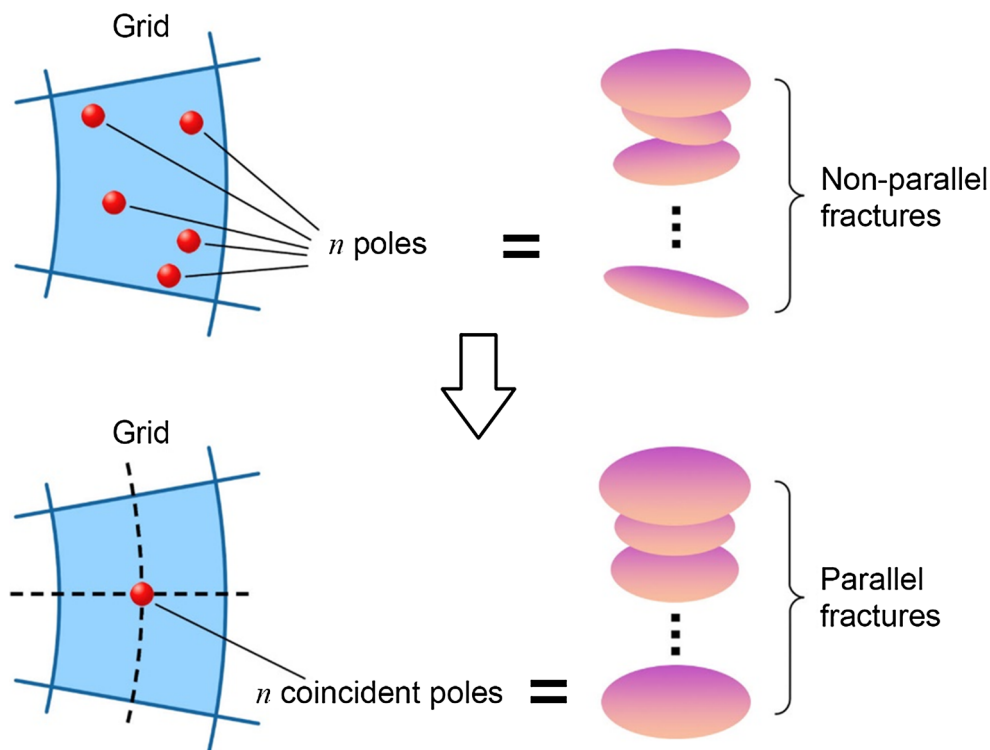
**Fig. 4** Spatial geometric interpretation of the estimation error involved in the Terzaghi estimator

Secondly, using the specified parameters, the DFN model in 3D was generated using a stochastic modeling technique. The fracture geometry in this technique is characterized by the Baecher et al. (1977) disk model, which is defined with a center location, radius, orientation, and aperture. This model makes various assumptions: (1) the fractures are disk shaped, (2) the aperture is a mutually independent variable, (3) the radius is a mutually independent variable, (4) the orientation is also a mutually independent variable, and (5) the radius and orientation are independent of each other. For simplicity, the roughness feature is not considered in the modeling. This technique used Monte Carlo operations to generate random numbers of geometric elements in the desired distributions/processes and the subsequent 3D simulations for visualizing the network. Here, scanlines with individual directions (as listed in Table 1) were separately incorporated into the model to produce seven intersection angles, and exposures on the model were created to coordinate with scanlines, as depicted in Fig. 6. Observations of fracture orientations were performed along the scanlines on these exposures. In each model, the orientations were observed separately under six global sample densities, as listed in Table 1, which resulted in various sample sizes. Thus, for the seven models, 42 samples in 1D were observed, and they all fell into the region of interest outside the blind zone. Figure 7 shows a selection of observed 1D distributions.

Finally, 3D distributions were estimated from the observed 1D frequencies, using the Terzaghi estimator under four grid size settings: $1° × 1°$, $2° × 2°$, $5° × 5°$ and $10° × 10°$. (For lack of space, the estimated 3D distributions are not presented herein.) The statistical difference between true and estimated 3D distributions was then evaluated, using the two-dimensional Kolmogorov–Smirnov test, and the results are presented in the following section, where the relationship between this statistical difference and parameter grid size will be further analyzed. In addition, the particular grid size giving the smallest statistical difference will be identified as the optimal parameter setting of the Terzaghi estimator.

3.2 Analysis Results

3.2.1 Accuracy of the Terzaghi Estimator Outside the Blind Zone

The statistics on the significance from 168 conditions (Fig. 8) illustrates that all significance values are less than or equal to 0.81, and the upper limit of the 95% confidence intervals does not exceed 0.75 and is far below 1. This result indicates that the Terzaghi estimate of the 3D distribution has a significant statistical distance from the true 3D distribution, implying that the Terzaghi estimator does not permit an extremely accurate estimate when applied
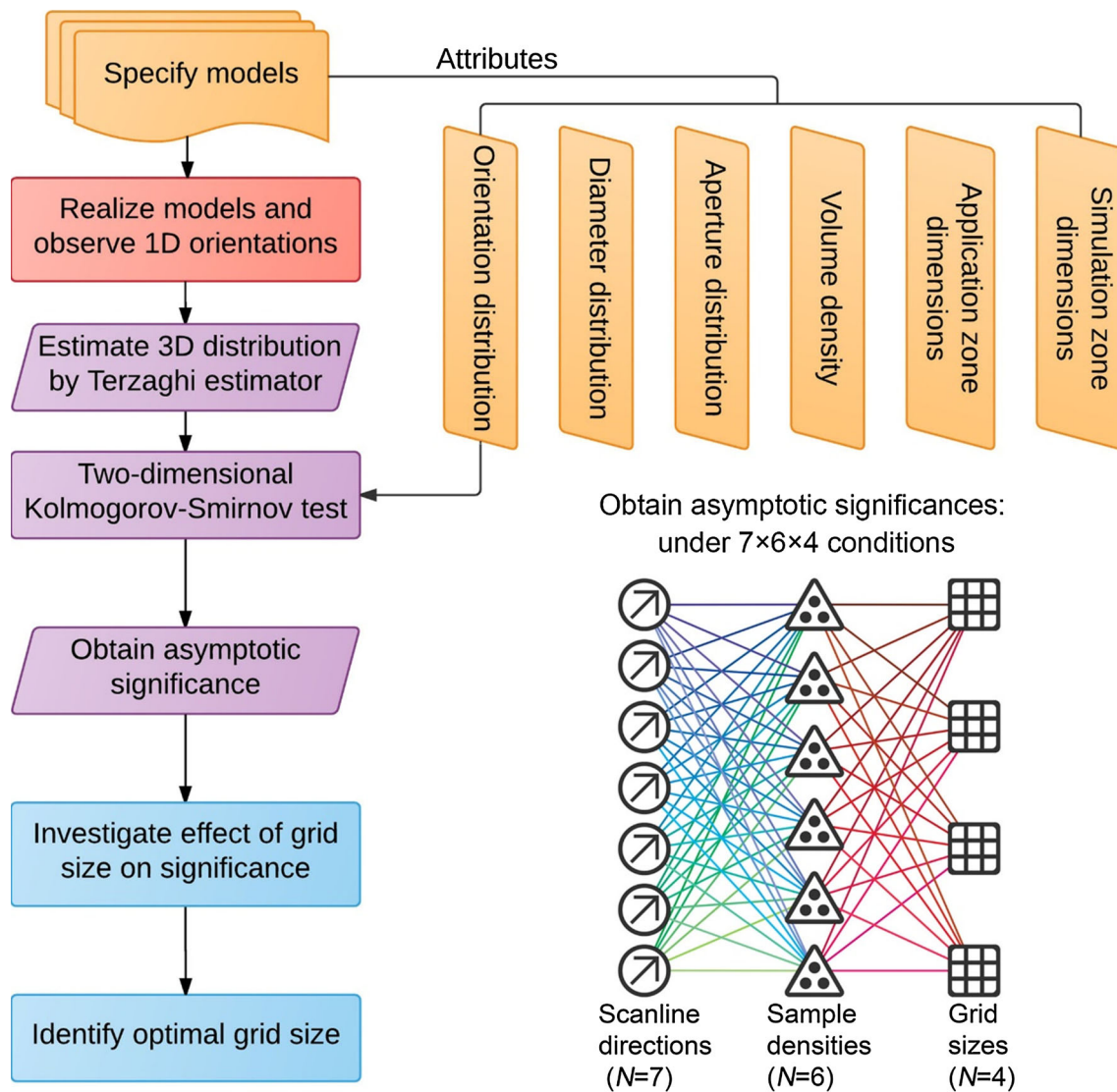
Fig. 5 Simulation workflow. There are three primary steps for investigating the effect of grid size on accuracy and identifying the particular grid size with the highest accuracy: (1) specification of model parameters, (2) realization of models and 1D orientation observations, and (3) estimation of 3D orientation distribution from 1D observations and asymptotic significance evaluations

outside the blind zone. Seriously low significances are detected in certain cases of low global sample density and huge grid sizes, suggesting that the Terzaghi estimator suffers significant inaccuracy when applied in these cases.

The upper limit of the 95% confidence interval of significances over intersection angles (as shown in Fig. 8a) indicates that the significance increases slightly by 0.07 as the intersection angle increases from nearly 50° to 89°. This result suggests that accuracy improvements are limited when the scanline shifts to be orthogonal to fractures, although this orthogonality was widely suggested (Dockrill and Shipton 2010; Park and West 2002). The upper limit of the 95% confidence interval of significances over global sample densities (as shown in Fig. 8b) indicates that the significance increase (0.37) is considerable when the global sample density rises from 0.05 to $0.5^{\circ-2}$. Therefore, the

orientation sample size should be enlarged in field surveys of fracture geometry when possible. The upper limit of the 95% confidence interval of significances over grid sizes (as shown in Fig. 8c) indicates that the significance does not show a steady variation trend as the grid size changes. A comprehensive analysis of the effect of grid size will be included in the following section.

3.2.2 Effect of Grid Size on the Accuracy and Identification of Optimal Grid Size

The significance values obtained by the test are shown in Fig. 9. For most sample densities and intersection angles, the significance shows an increasing function of grid size in the size interval between 1° × 1° and 2° × 2°, a decreasing function between 2° × 2° and 5° × 5°, and a constant

Table 1 Parameter specification for DFN modeling and orientation observations

Parameter	Specification
Geometry of fracture	Baecher disk model
Dimensions of simulated zone[a]: length (m) × width (m) × height (m)	20 × 20 × 20
Dimensions of applied zone[b]: length (m) × width (m) × height (m)	10 × 10 × 10
Distribution of center location	*Poisson* (5)[c]
Distribution of orientation: dip direction/angle (°)	*U* (175, 185)[d]/*U* (40, 50)
Distribution of radius (m)	*Exp* (1)[e]
Distribution of aperture (mm)	*Exp* (3)
Direction of scanline: trend/plunge (°)	000/45
	010/45
	020/45
	030/45
	040/45
	050/45
	060/45
Global sample density (°$^{-2}$)	0.05
	0.1
	0.2
	0.3
	0.4
	0.5

[a] Simulated zone = 3D region where the simulation of fractures occurs

[b] Applied zone = 3D region where sampling of fractures and observations is performed

[c] *Poisson* (λ) = spatial Poisson point distribution, where λ is the volume density (m^{-3}) defined by the number of fracture centers per rock volume

[d] *U* (*m*, *n*) = uniform distribution, where *m* is the lower limit and *n* is the upper limit

[e] *Exp* (*k*) = exponential distribution, where *k* is the reciprocal of the mean

function between $5° × 5°$ and $10° × 10°$. This result suggests that grid size affects accuracy. Specifically, (a) decreasing the grid size from $10° × 10°$ to $5° × 5°$ cannot stimulate accuracy improvements, (b) decreasing the grid size from $5° × 5°$ to $2° × 2°$ improves accuracy, and (c) decreasing the grid size from $2° × 2°$ to $1° × 1°$ leads to a drop in accuracy.

Peak significance occurs at a grid size of $2° × 2°$ for most sample densities and intersection angles, although in certain cases where the global sample density is $0.5°^{-2}$, this grid size does not achieve peak significance. Thus, $2° × 2°$ is identified as the optimal grid size. But additionally notable is that for cases where the global sample density exceeds $0.5°^{-2}$, the optimal grid size is $1° × 1°$.

4 Verification with a Natural Fracture Case

The effect of grid size on accuracy, as well as the optimal grid size, is verified with an actual case of natural fractures from a rocky roadcut outcrop near the 2008 Wenchuan earthquake epicenter. The verification process is as follows: (1) 1D fracture orientations were observed in the field by the scanline mapping technique. (2) 3D distributions were estimated from the 1D observations using the Terzaghi estimator, and various grid sizes were applied. (3) 3D fracture networks were reproduced via the stochastic modeling technique using the estimated 3D distributions of orientation. In these reproduced networks, scanlines in the field were reconstructed, and the fractures intersected by these scanlines were observed. To differentiate the fracture orientations observed in the field, the fractures observed on the reproduced model are referred to as reproduced 1D orientations. (4) The statistical differences between the two data sets (observed and reproduced 1D orientations) were evaluated at a range of grid sizes using the two-dimensional Kolmogorov–Smirnov test. The process is presented in detail in the following section.

4.1 1D Orientation Observations, 3D Distribution Estimations, Modeling and Testing

The field site is a rocky roadcut outcrop located near the town of Yingxiu (Fig. 10a). The rock has two fracture sets,

Fig. 6 DFN models in 3D. The scanline for mapping is at the trend/plunge of **a** 000/45°; **b** 010/45°; **c** 020/45°; **d** 030/45°; **e** 040/45°; **f** 050/45°; and **g** 060/45°
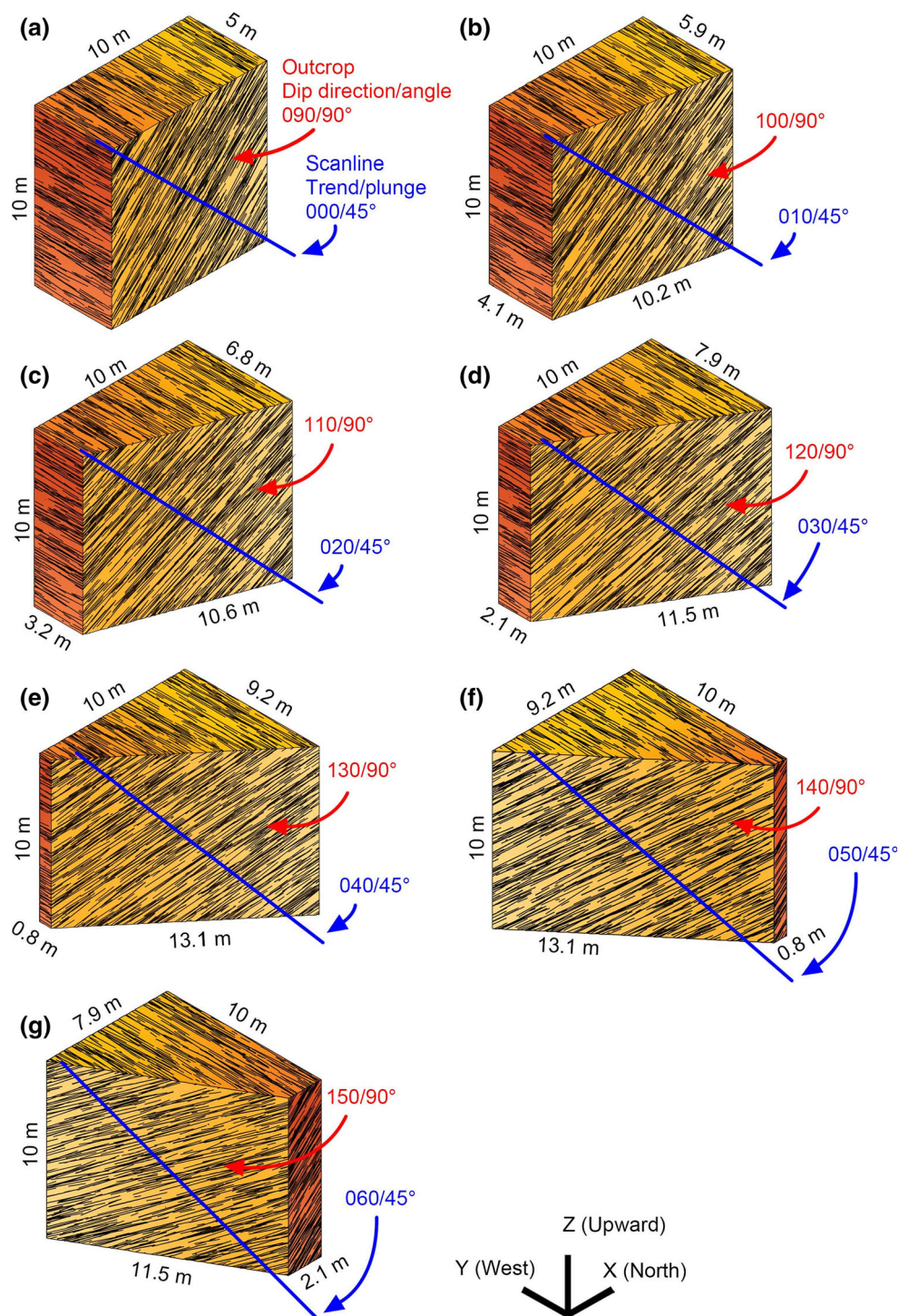

and one is a set of bedding planes. A scanline with a trend/plunge of 108/15° was fixed on the outcrop to map the 1D bedding plane geometries (Fig. 10b). The observed 1D orientations are shown in Fig. 11a, which also shows the scanline direction and region of interest outside the resulting blind zone. It is apparent from this figure that the fracture orientations all lie in the region of interest outside the blind zone.

The 3D distribution was estimated from 1D observations using the Terzaghi estimator. To verify the effect of grid size, the estimations were performed with four grid sizes (1° × 1°, 2° × 2°, 5° × 5° and 10° × 10°) in combination with four global sample densities: 0.02, 0.05, 0.1, and $0.2^{\circ-2}$. Figure 11b shows only the 3D distribution, estimated under a combination of 5° × 5° grid size and $0.2^{\circ-2}$ global sample density. Other parameters necessary for

Fig. 7 Observed 1D orientations presented in terms of pole diagrams (experiment). The scanline for mapping is at the trend/plunge of **a** 000/45°; **b** 010/45°; **c** 020/45°; **d** 030/45°; **e** 040/45°; **f** 050/45°; and **g** 060/45°

Springer
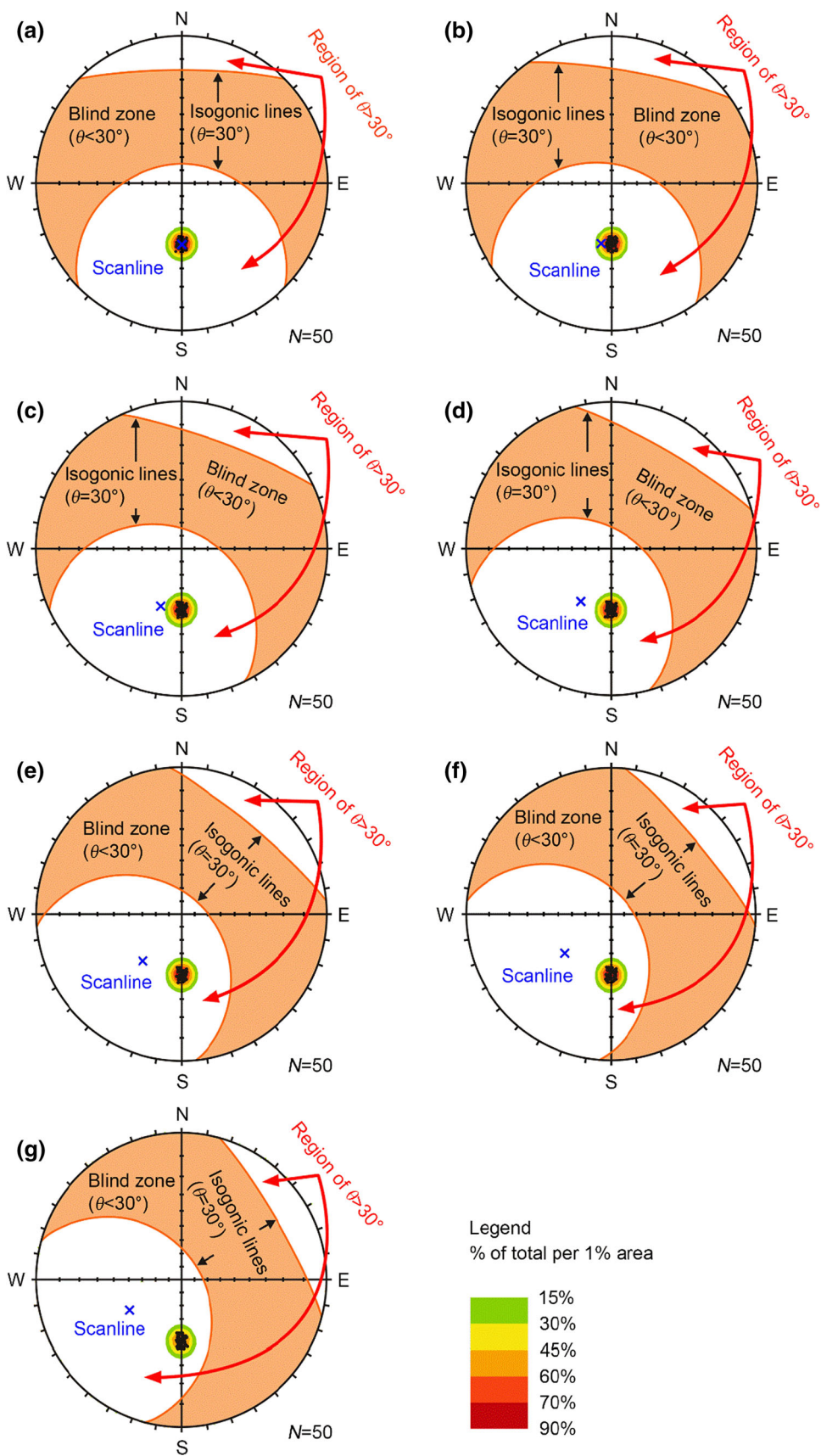
Fig. 8 Scatter plots of significance for 168 conditions, accompanied by the 95% confidence interval (*blue line*). **a** Significance versus intersection angle, **b** significance versus global sample density, **c** significance versus grid size
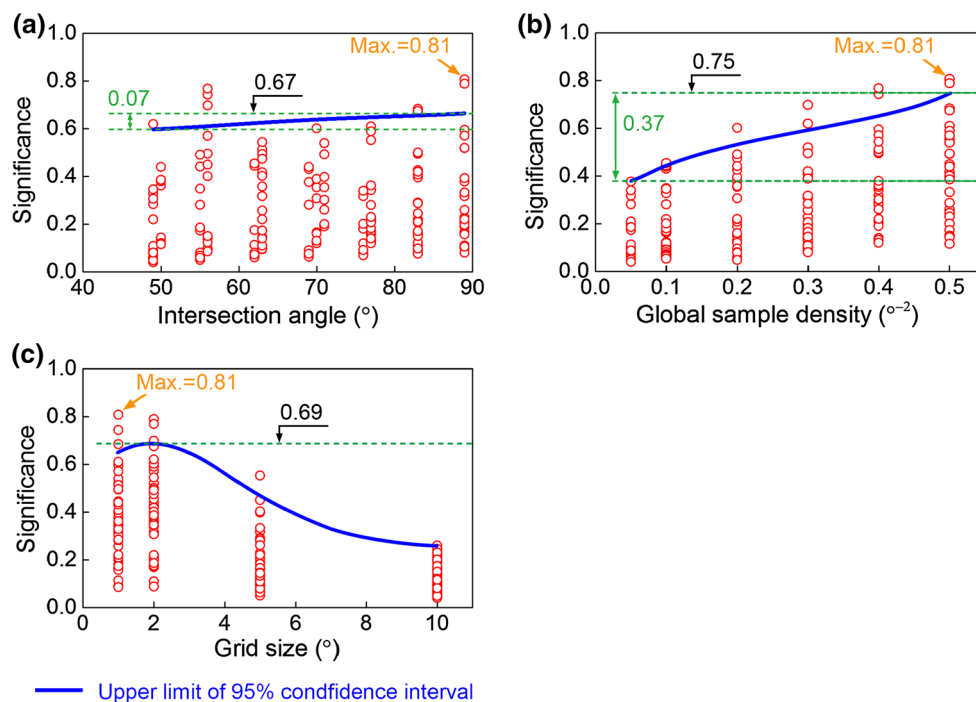
modeling were also calculated, and the results are listed in Table 2. Using these parameters, DFNs were reproduced, together with the scanline (as depicted in Fig. 11c). In the reproduced models, orientations of those fractures intersected by the scanline (reproduced 1D observations) were measured, with sample sizes equal to that in the field. Figure 11d shows one of the reproduced 1D orientation distributions. The statistical difference between the observed and reproduced 1D observations was evaluated using the two-dimensional Kolmogorov–Smirnov test, and those evaluation results are shown in the following section.
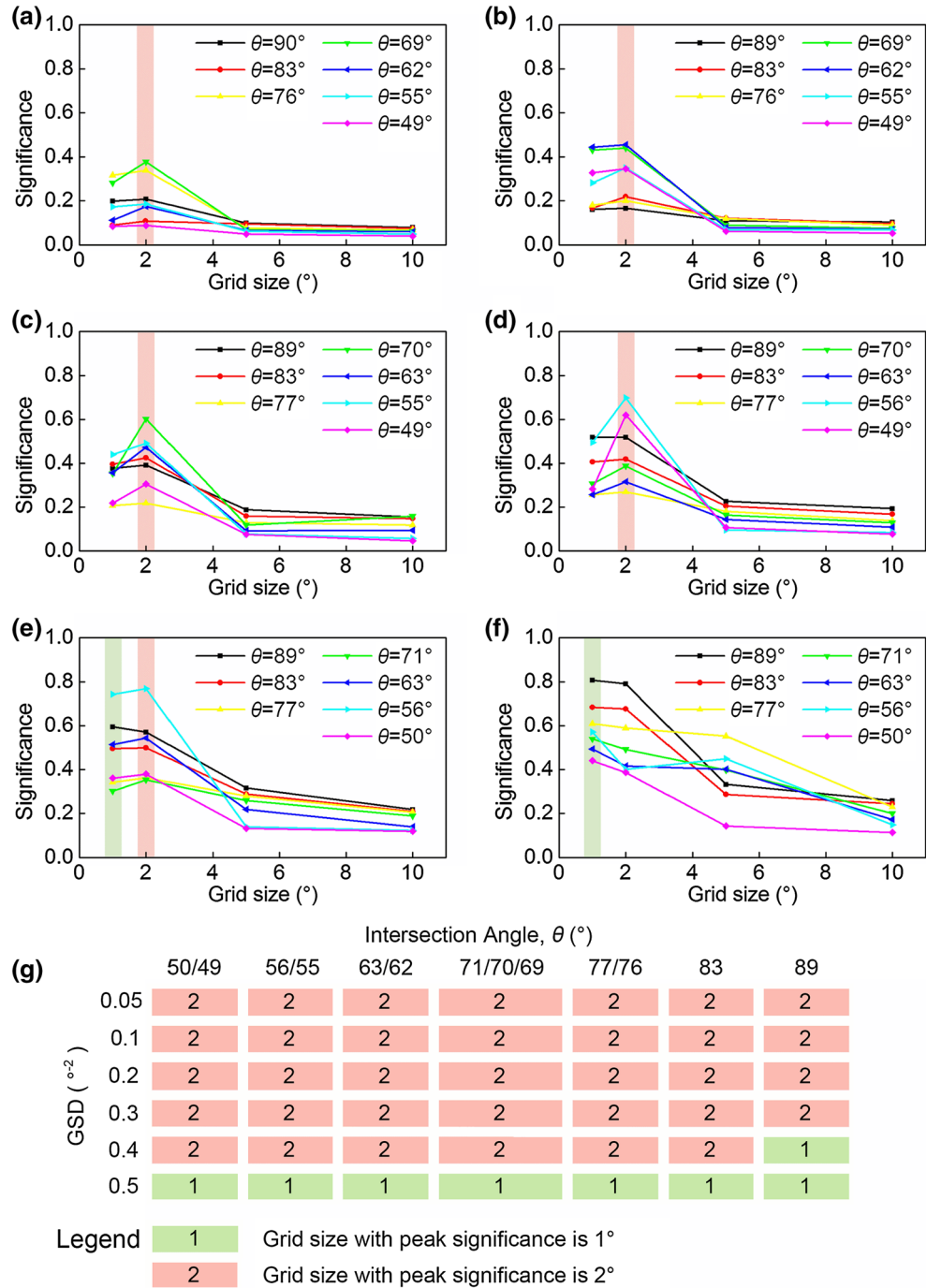
4.2 Verification Result

The significance values are less than 1, and when the grid size exceeds $5° \times 5°$, the significance values are extremely small. This empirical result supports the relevant findings derived from the analysis of simulated data. Figure 12 shows the significance values over grid sizes. The curve indicates that the significance is an increasing function of grid size in the size interval between $1° \times 1°$ and $2° \times 2°$, decreasing function of grid size between $2° \times 2°$ and $5° \times 5°$, and approximately constant function of grid size between $5° \times 5°$ and $10° \times 10°$. Moreover, the peak of significance appears at the grid size of $2° \times 2°$. The two results are consistent with the simulated analysis findings regarding the effect of grid size and optimal grid size.

Theoretical derivation of the Terzaghi equation (Sect. 2) suggests that a smaller grid size is supposed to contribute to higher estimation accuracy. For grid sizes greater than

$2° \times 2°$, accuracy appears to increase as the grid size shrinks, whereas for grid sizes smaller than $2° \times 2°$, accuracy decreases as the grid size shrinks, as detected in the numerical and empirical cases (Figs. 9, 12). How can the apparent variation and partial inconsistency between the theoretical result and the numerical/empirical case be accounted for? A twofold effect of grid size on accuracy likely occurs: (1) a positive (direct) effect and (2) a negative (indirect) effect. Shrinking the grid size, which is detailed in Sect. 2, would reduce the error of the Riemann middle sum, thereby directly benefitting accuracy improvements (positive effect). However, shrinking the grid size will cause smaller sample numbers to fall into individual grids, thereby increasing the likelihood of larger sampling errors. Such errors would transfer to the estimation result (negative effect). When the positive effect exceeds the negative effect, the resulting appearance of superposition demonstrates that accuracy increases as the grid size shrinks (i.e., when greater than the critical grid size of $2° \times 2°$) and decreases otherwise (i.e., when less than the critical grid size of $2° \times 2°$). For global sample densities no more than $0.5°^{-2}$, the critical grid size mostly occurs at $2° \times 2°$, whereas for global sample densities higher than $0.5°^{-2}$, the critical grid size appears to be $1° \times 1°$, as found in this work. This high global sample density is responsible for the change in critical grid size because it leads to more individuals falling into grids, which weakens the negative effect. Compared with the case of global sample densities that are no more than $0.5°^{-2}$, the negative effect in the global sample density of $0.5°^{-2}$ does

Fig. 9 Significance versus grid size and the statistics for the grid sizes with peak significance. Significance values were tested using the two-dimensional Kolmogorov–Smirnov test. Significance versus grid size curves under the global sample densities of **a** $0.05^{\circ-2}$; **b** $0.1^{\circ-2}$; **c** $0.2^{\circ-2}$; **d** $0.3^{\circ-2}$; **e** $0.4^{\circ-2}$; and **f** $0.5^{\circ-2}$. **g** Statistics for grid sizes with peak significance. The cells show the grid sizes with peak significance versus the intersection angle and global sample density (GSD)
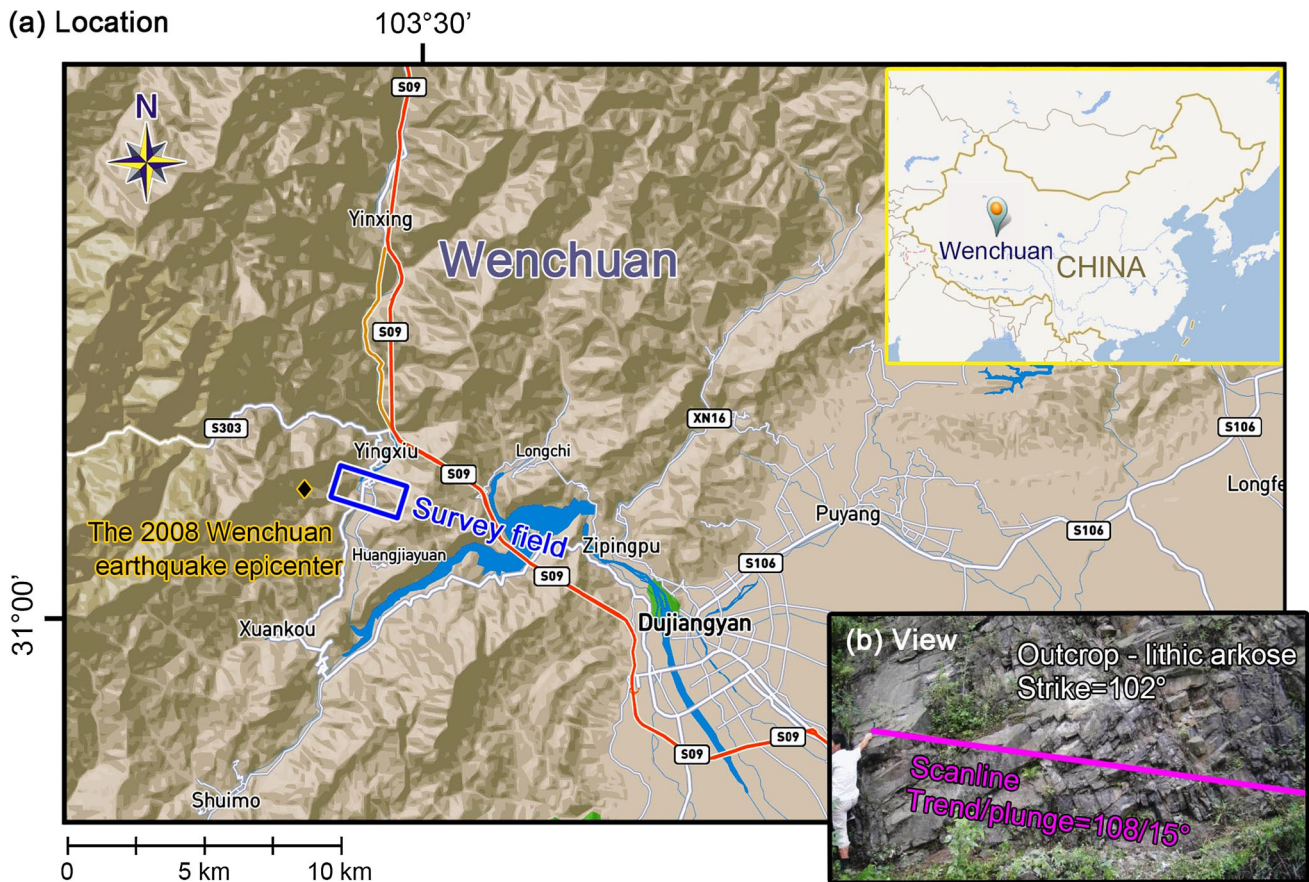

5 Discussion

The 3D orientation distribution estimated using the Terzaghi estimator is an important input parameter for DFN modeling and has a significant application in oil production evaluation and carbon sequestration operations. The use of the suggested optimal grid size of $2° \times 2°$ in the estimator has been demonstrated to provide a more accurate estimate of 3D orientation distributions than other grid sizes in the vast majority of cases, thereby producing a DFN geometrical model that accurately represents the 3D fracture population. Hence, we recommend that prior to modeling, the observed 1D distribution should be corrected, preferably under the optimal setting of a $2° \times 2°$ grid size.

not exceed the positive effect, even when grid sizes are smaller than $2° \times 2°$. Therefore, the grid size of $1° \times 1°$ exhibits maximum accuracy in this case.

Fig. 10 a Location of the survey field. The site is near the town of Yingxiu in Wenchuan, Sichuan Province, China, approximately 1800 m east of the 2008 Wenchuan earthquake epicenter. **b** View of the survey field. This nearly vertical outcrop (11 m long, 5 m wide, and 6 m high) strikes at 102° and develops in the upper Triassic lithic arkose of the Xujiahe Formation

Previous studies performing DFN modeling usually input the observed 1D orientation distribution directly (Fereshtenejad et al. 2016; Maffucci et al. 2015; Panza et al. 2016; Tsang et al. 2015) or the 3D distribution estimated using the Terzaghi estimator under an arbitrary grid size (Desbarats et al. 1999; Keren and Kirkpatrick 2016; Stephens et al. 2015). Comparing the Terzaghi 3D estimate and a field survey, researchers have found that estimates with intersection angles no more than 20° or 30° cannot reflect the true distribution in 3D, and this angle interval is defined as the blind zone (Park and West 2002). Those summaries are based on an underlying assumption that the field survey captures the true 3D distribution. Unfortunately, the 3D distribution presents access limitations, rendering direct validation of the representation essentially impossible. In this paper, the 30° blind zone drawn from this assumption is applied to focus on investigating the accuracy rather than estimating the blind zone and avoid a longer discussion of the precise boundary of the blind zone.

Qualitative analyses, such as those by Fouché and Diebolt (2004), Martel (1999) and Munn (2012), have implied that the estimation accuracy of the Terzaghi

estimator is higher when applied outside the blind zone. To date, no quantitative study has been performed to evaluate the accuracy of the Terzaghi estimation. The validity of accuracy investigations based on comparisons between estimates and field surveys is questionable because of the unconfirmed assumption, as previously noted, although the investigation of Park and West (2002) appeared to involve this assumption. In this paper, we present an investigation employing simulated fractures where the true orientation distribution can be accurately established; thus, comparisons can be made between the true and estimated 3D distributions. More precisely, when the true orientation distribution is accurately known, the true and estimated 3D distributions can be compared. Although the true distribution is not known in the actual case of natural fractures, the Terzaghi estimator accuracy is investigated by comparing observed and reproduced 1D orientations, as performed in the case study in this work. The statistical difference obtained via this approach indirectly reflects the statistical difference between the true and estimated 3D distributions. The investigation herein does not involve the assumption that the field survey captures the true 3D
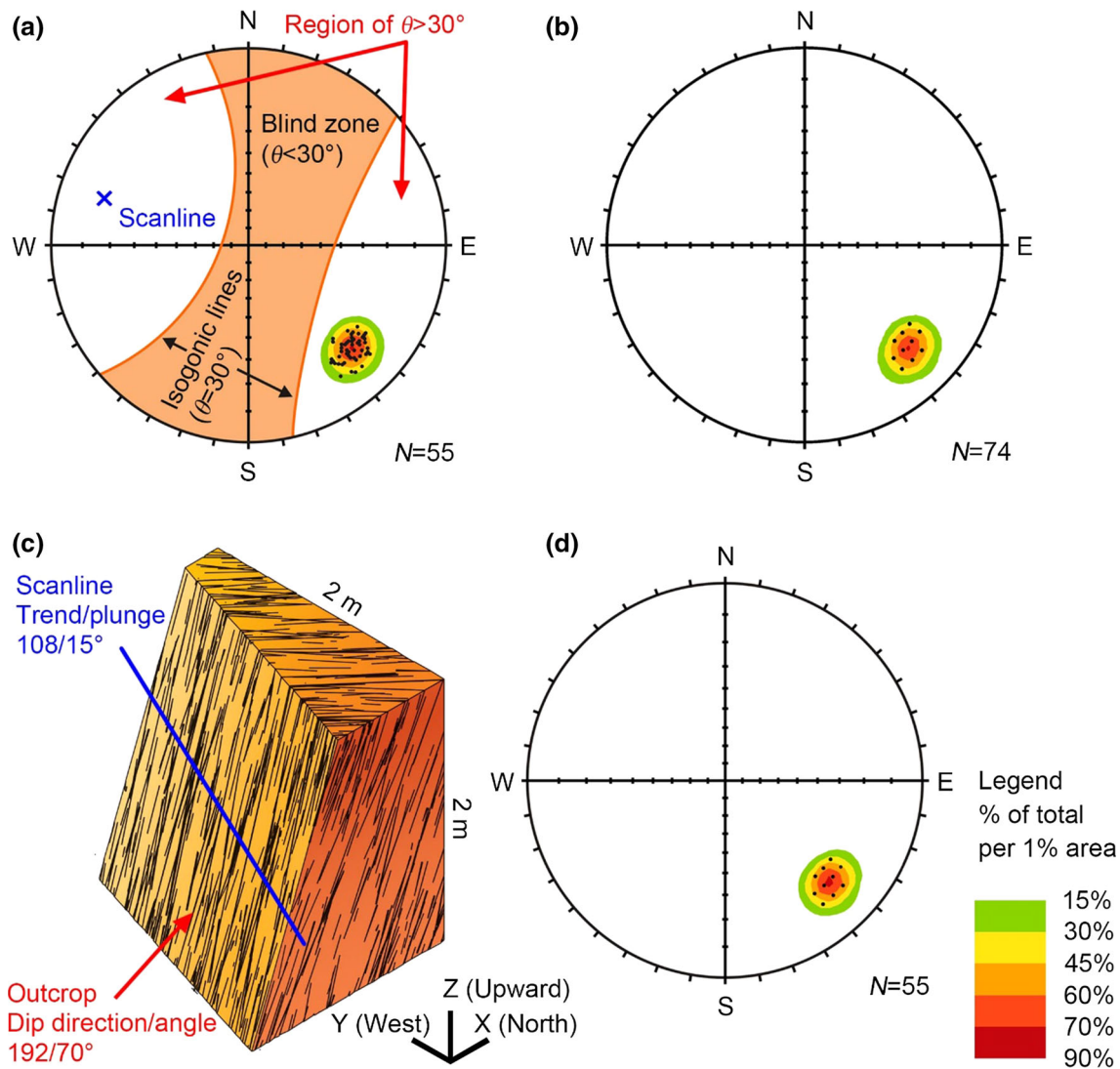
Fig. 11 a Observed 1D orientations, accompanied by the scanline direction and region of interest outside the resulting blind zone (case). **b** Orientations in 3D estimated under the combination of a grid size of $5° \times 5°$ and a global sample density of $0.2°^{-2}$. Note that because certain poles coincide, it seems there are only 11 poles. In fact, there are 74 poles. **c** DFN model in 3D, which adopts the 3D orientation distribution estimated under the combination of $5° \times 5°$ grid size and $0.2°^{-2}$ global sample density. **d** Reproduced 1D orientations that correspond to the 3D orientation distribution estimated under the combination of $5° \times 5°$ grid size and $0.2°^{-2}$ global sample density

Table 2 Parameter specification for DFN modeling and orientation observations. Distributions of the orientation are expressed in terms of frequency data, as shown in Fig. 11b, and are not duplicated here

Parameter	Specification
Geometry of fracture	Baecher disk model
Dimensions of simulated zone: length (m) × width (m) × height (m)	$20 \times 20 \times 20$
Dimensions of applied zone: length (m) × width (m) × height (m)	$10 \times 10 \times 10$
Distribution of center location	*Poisson* (4)
Distribution of radius (m)	*Exp* (0.25)
Distribution of aperture (mm)	*Exp* (3.2)
Direction of scanline: trend/plunge (°)	108/15
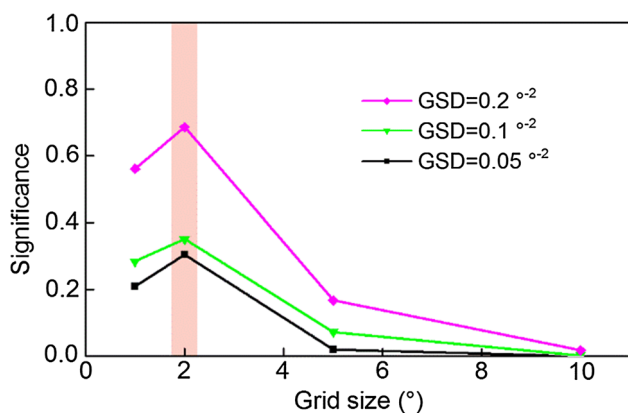
Fig. 12 Significance versus grid size. The significances are tested using the two-dimensional Kolmogorov–Smirnov test under three global sample densities (GSDs)

distribution and is consequently more rigorous, relative to past investigations that have directly compared Terzaghi estimates and field surveys. Such an investigation strategy provides a practical method of accurately analyzing fracture geometry, and the results will also benefit studies relevant to 3D distribution estimations, including future assessments of the blind zone.

The findings in this work come from scanline surveys, and their applicability to borehole/well data remains unclear. Scanlines are a sampling tool in which the width is negligible relative to the fracture size. In contrast, boreholes/wells with a sizeable width differ from scanlines. Thus, the applicability of the findings (derived from the scanline situation) to borehole/well conditions should be empirically examined when adequate orientation data from boreholes/wells are available. Alternatively, an investigation could be performed to address the width effect of the sampling tool on applicability. If the investigation results showed the width had no effect, then findings based on the scanline will hold true under borehole/well conditions. Mauldon and Mauldon (1997) provided some general mathematical results about the width effect on the estimation accuracy. However, the additional empirical investigations with actual data can provide insight. In addition, a systematic analysis for different cases (e.g., intersection angles, global sample densities, and grid sizes) is desirable. Finally, the impact of grid size on the estimation accuracy, including the optimal grid size value, is valuable.

6 Conclusions

In this study, a detailed, rigorous mathematical derivation of the Terzaghi equation generated a theoretical, qualitative proof that the Terzaghi estimator using the Riemann

middle sum tends to have an estimation error. This error affects the estimate of 3D orientation distributions when applied outside the blind zone. An alternative interpretation of the error from a spatial geometric perspective is that nonparallel fractures within individual grids are incorrectly defined as parallel fractures with a uniform central orientation. These findings provide deeper insights into the Terzaghi estimator.

Quantitative surveys have demonstrated that the Terzaghi estimate of 3D orientation distribution is statistically significantly different from the true 3D distribution. Consequently, the Terzaghi estimator does not provide an extremely accurate estimate when applied outside the blind zone and may even result in seriously low accuracy ranges in cases of narrow intersection angles, low global sample densities, and large grid sizes. Intersection angle widening does not produce a significant accuracy improvement, but increasing the sample size does improve the accuracy of the estimator.

In addition, the effect of grid size on accuracy was systematically investigated, and we found that (a) decreasing the grid size from $10° \times 10°$ to $5° \times 5°$ does not improve the accuracy, (b) decreasing the grid size from $5° \times 5°$ to $2° \times 2°$ improves the accuracy, and (c) decreasing the grid size from $2° \times 2°$ to $1° \times 1°$ reduces the accuracy. In this investigation, the particular grid size of $2° \times 2°$ was identified as the optimal parameter setting of the Terzaghi estimator and was recommended to improve the accuracy. However, if the global sample density reaches $0.5°^{-2}$, the maximum accuracy tends to occur at $1° \times 1°$.

References

Baecher G, Lanney N, Einstein H (1977) Statistical description of rock properties and sampling. Paper presented at the 18th US symposium on rock mechanics (USRMS). American Rock Mechanics Association

Chaminé HI, Afonso MJ, Ramos L, Pinheiro R (2014) Scanline sampling techniques for rock engineering surveys: insights from intrinsic geologic variability and uncertainty. In: Lollino G, Giordan D, Thuro K, Carranza-Torres C, Wu F, Marinos P, Delgado C (eds) Engineering geology for society and territory. Springer, Cham, pp 357–361

Clair J, Moon S, Holbrook WS, Perron JT, Riebe CS, Martel SJ, Carr B, Harman C, Singha K, Richter DD (2015) Geophysical imaging reveals topographic stress control of bedrock weathering. Science 350(6260):534–538. doi:10.1126/science.aab2210

Desbarats AJ, Boyle DR, Stapinsky M, Robin MJL (1999) A dual-porosity model for water level response to atmospheric loading

in wells tapping fractured rock aquifers. Water Resour Res 35(5):1495–1505. doi:10.1029/1998wr900119

Dockrill B, Shipton ZK (2010) Structural controls on leakage from a natural CO_2 geologic storage site: Central Utah, U.S.A. J Struct Geol 32(11):1768–1782. doi:10.1016/j.jsg.2010.01.007

Fereshtenejad S, Afshari MK, Bafghi AY, Laderian A, Safaei H, Song JJ (2016) A discrete fracture network model for geometrical modeling of cylindrically folded rock layers. Eng Geol 215:81–90. doi:10.1016/j.enggeo.2016.11.004

Fernandes AJ, Maldaner CH, Negri F, Rouleau A, Wahnfried ID (2016) Aspects of a conceptual groundwater flow model of the Serra Geral basalt aquifer (Sao Paulo, Brazil) from physical and structural geology data. Hydrogeol J 24:1199–1212. doi:10.1007/s10040-016-1370-6

Fisher JE, Shakoor A, Watts CF (2014) Comparing discontinuity orientation data collected by terrestrial LiDAR and transit compass methods. Eng Geol 181:78–92. doi:10.1016/j.enggeo.2014.08.014

Fouché O, Diebolt J (2004) Describing the geometry of 3D fracture systems by correcting for linear sampling bias. Math Geol 36(1):33–63. doi:10.1023/b:matg.0000016229.37309.fd

Gao M, Jin W, Zhang R, Xie J, Yu B, Duan H (2016) Fracture size estimation using data from multiple boreholes. Int J Rock Mech Min Sci 86:29–41. doi:10.1016/j.ijrmms.2016.04.005

Ghislain T, Rishi P, Clément D, Lucille C, Pauline V, Sébastien P (2016) Properties of a pair of fracture networks produced by triaxial deformation experiments: insights on fluid flow using discrete fracture network models. Hydrogeol J. doi:10.1007/s10040-016-1468-x

Goodman RE (1976) Methods of geological engineering in discontinuous rocks. West Publishing Co, St. Paul

Haftani M, Chehreh HA, Mehinrad A, Binazadeh K (2016) Practical investigations on use of weighted joint density to decrease the limitations of RQD measurements. Rock Mech Rock Eng 49(4):1551–1558. doi:10.1007/s00603-015-0788-9

Han X, Chen J, Wang Q, Li Y, Zhang W, Yu T (2016) A 3D fracture network model for the undisturbed rock mass at the Songta dam site based on small samples. Rock Mech Rock Eng 49(2):611–619. doi:10.1007/s00603-015-0747-5

Havaej M, Coggan J, Stead D, Elmo D (2016) A combined remote sensing–numerical modelling approach to the stability analysis of Delabole Slate Quarry, Cornwall, UK. Rock Mech Rock Eng 49(4):1227–1245. doi:10.1007/s00603-015-0805-z

Huang L, Tang H, Tan Q, Wang D, Wang L, Ez Eldin MAM, Li C, Wu Q (2016) A novel method for correcting scanline-observational bias of discontinuity orientation. Sci Rep 6:22942. doi:10.1038/srep22942

Justel A, Peña D, Zamar R (1997) A multivariate Kolmogorov–Smirnov test of goodness of fit. Stat Probab Lett 35(3):251–259. doi:10.1016/s0167-7152(97)00020-5

Keren TT, Kirkpatrick JD (2016) The damage is done: low fault friction recorded in the damage zone of the shallow Japan Trench décollement. J Geophys Res Solid Earth 121(5):3804–3824. doi:10.1002/2015jb012311

Kinney JJ (2015) Probability: an introduction with statistical applications. Wiley, Hoboken

Lopes RH (2010) Kolmogorov–Smirnov test. In: Lovric M (ed) International encyclopedia of statistical science. Springer, Berlin, pp 718–720

Lopes RH, Reid I, Hobson PR (2007) The two-dimensional Kolmogorov–Smirnov test. Paper presented at XI international workshop on advanced computing and analysis techniques in physics research, proceedings of science, Amsterdam, Netherlands

Maffucci R, Bigi S, Corrado S, Chiodi A, di Paolo L, Giordano G, Invernizzi C (2015) Quality assessment of reservoirs by means

of outcrop data and "discrete fracture network" models: the case history of Rosario de La Frontera (NW Argentina) geothermal system. Tectonophysics 647–648:112–131. doi:10.1016/j.tecto.2015.02.016

Martel SJ (1999) Analysis of fracture orientation data from boreholes. Environ Eng Geosci V(2):213–233. doi:10.2113/gseegeosci.v.2.213

Martin MW, Tannant DD (2004) A technique for identifying structural domain boundaries at the EKATI Diamond Mine. Eng Geol 74(3–4):247–264. doi:10.1016/j.enggeo.2004.04.001

Mauldon M (1998) Estimating mean fracture trace length and density from observations in convex windows. Rock Mech Rock Eng 31(4):201–216. doi:10.1007/s006030050021

Mauldon M, Mauldon JG (1997) Fracture sampling on a cylinder: from scanlines to boreholes and tunnels. Rock Mech Rock Eng 30(3):129–144. doi:10.1007/bf01047389

Mauldon M, Dunne WM, Rohrbaugh MB (2001) Circular scanlines and circular windows: new tools for characterizing the geometry of fracture traces. J Struct Geol 23(2):247–258. doi:10.1016/s0191-8141(00)00094-8

Middleton RS, Carey JW, Currier RP, Hyman JD, Kang Q, Karra S, Jiménez-Martínez J, Porter ML, Viswanathan HS (2015) Shale gas and non-aqueous fracturing fluids: opportunities and challenges for supercritical CO_2. Appl Energy 147:500–509. doi:10.1016/j.apenergy.2015.03.023

Munn J (2012) High-resolution discrete fracture network characterization using inclined coreholes in a Silurian dolostone aquifer in Guelph, Ontario. Dissertation, University of Guelph

Nur A, Booker JR (1972) Aftershocks caused by pore fluid flow? Science 175(4024):885–887. doi:10.1126/science.175.4024.885

Pandey SN, Chaudhuri A, Kelkar S (2017) A coupled thermo-hydro-mechanical modeling of fracture aperture alteration and reservoir deformation during heat extraction from a geothermal reservoir. Geothermics 65:17–31. doi:10.1016/j.geothermics.2016.08.006

Panza E, Agosta F, Rustichelli A, Zambrano M, Tondi E, Prosser G, Giorgioni M, Janiseck JM (2016) Fracture stratigraphy and fluid flow properties of shallow-water, tight carbonates: the case study of the Murge Plateau (southern Italy). Mar Pet Geol 73:350–370. doi:10.1016/j.marpetgeo.2016.03.022

Park HJ, West TR (2002) Sampling bias of discontinuity orientation caused by linear sampling technique. Eng Geol 66(1–2):99–110. doi:10.1016/s0013-7952(02)00034-0

Peterson JK (2016) Riemann integration. In: Peterson JK (ed) Calculus for cognitive scientists. Springer, Singapore, pp 129–164

Priest SD (1985) Hemispherical projection methods in rock mechanics. George Allen and Unwin, London

Priest SD (2012) Discontinuity analysis for rock engineering. Springer, Cham

Stephens MB, Follin S, Petersson J, Isaksson H, Juhlin C, Simeonov A (2015) Review of the deterministic modelling of deformation zones and fracture domains at the site proposed for a spent nuclear fuel repository, Sweden, and consequences of structural anisotropy. Tectonophysics 653:68–94. doi:10.1016/j.tecto.2015.03.027

Terzaghi RD (1965) Sources of error in joint surveys. Géotechnique 15(3):287–304. doi:10.1680/geot.1965.15.3.287

Tsang CF, Neretnieks I, Tsang Y (2015) Hydrologic issues associated with nuclear waste repositories. Water Resour Res 51(9):6923–6972. doi:10.1002/2015wr017641

Yow J (1987) Blind zones in the acquisition of discontinuity orientation data. Int J Rock Mech Min Sci Geomech Abstr 24(5):317–318. doi:10.1118/1.3664003